The Status of the Tropical Rainfall Measuring Mission (TRMM) after Two Years in Orbit

C. KUMMEROW,[a,*] J. SIMPSON,[a] O. THIELE,[a] W. BARNES,[a] A. T. C. CHANG,[a] E. STOCKER,[a] R. F. ADLER,[a] A. HOU,[a] R. KAKAR,[b] F. WENTZ,[c] P. ASHCROFT,[c] T. KOZU,[d] Y. HONG,[e] K. OKAMOTO,[f] T. IGUCHI,[f] H. KUROIWA,[f] E. IM,[g] Z. HADDAD,[g] G. HUFFMAN,[h] B. FERRIER,[i] W. S. OLSON,[i] E. ZIPSER,[j] E. A. SMITH,[k] T. T. WILHEIT,[l] G. NORTH,[l] T. KRISHNAMURTI,[m] AND K. NAKAMURA[n]

[a] *NASA Goddard Space Flight Center, Greenbelt, Maryland*
[b] *NASA Headquarters, Washington, District of Columbia*
[c] *Remote Sensing Systems, Santa Rosa, California*
[d] *Shimane University, Shimane, Japan*
[e] *The Aerospace Corporation, Los Angeles, California*
[f] *Communications Research Laboratory, Tokyo, Japan*
[g] *Jet Propulsion Laboratory, Pasadena, California*
[h] *Science Systems and Applications, Inc., Lanham, Maryland*
[i] *University of Maryland, Baltimore County, Baltimore, Maryland*
[j] *University of Utah, Salt Lake City, Utah*
[k] *NASA Marshall Space Flight Center, Huntsville, Alabama*
[l] *Texas A&M University, College Station, Texas*
[m] *The Florida State University, Tallahassee, Florida*
[n] *Nagoya University, Nagoya, Japan*

(Manuscript received 4 October 1999, in final form 20 June 2000)

ABSTRACT

The Tropical Rainfall Measuring Mission (TRMM) satellite was launched on 27 November 1997, and data from all the instruments first became available approximately 30 days after the launch. Since then, much progress has been made in the calibration of the sensors, the improvement of the rainfall algorithms, and applications of these results to areas such as data assimilation and model initialization. The TRMM Microwave Imager (TMI) calibration has been corrected and verified to account for a small source of radiation leaking into the TMI receiver. The precipitation radar calibration has been adjusted upward slightly (by 0.6 dBZ) to match better the ground reference targets; the visible and infrared sensor calibration remains largely unchanged. Two versions of the TRMM rainfall algorithms are discussed. The at-launch (version 4) algorithms showed differences of 40% when averaged over the global Tropics over 30-day periods. The improvements to the rainfall algorithms that were undertaken after launch are presented, and intercomparisons of these products (version 5) show agreement improving to 24% for global tropical monthly averages. The ground-based radar rainfall product generation is discussed. Quality-control issues have delayed the routine production of these products until the summer of 2000, but comparisons of TRMM products with early versions of the ground validation products as well as with rain gauge network data suggest that uncertainties among the TRMM algorithms are of approximately the same magnitude as differences between TRMM products and ground-based rainfall estimates. The TRMM field experiment program is discussed to describe active areas of measurements and plans to use these data for further algorithm improvements. In addition to the many papers in this special issue, results coming from the analysis of TRMM products to study the diurnal cycle, the climatological description of the vertical profile of precipitation, storm types, and the distribution of shallow convection, as well as advances in data assimilation of moisture and model forecast improvements using TRMM data, are discussed in a companion TRMM special issue in the *Journal of Climate* (1 December 2000, Vol. 13, No. 23).

1. Motivation and history of the Tropical Rainfall Measuring Mission (TRMM)

Tropical rainfall is important in the hydrological cycle and to the lives and welfare of humans. Three-fourths of the energy that drives the atmospheric wind circulation comes from the latent heat released by tropical precipitation. Precipitation, unfortunately, is one of the most difficult atmospheric parameters to measure because of the large variations in space and time. Tropical rainfall oscillates wildly between severe droughts and

* Current affiliation: Department of Atmospheric Science, Colorado State University, Fort Collins, Colorado.

Corresponding author address: Dr. Christian Kummerow, Dept. of Atmospheric Science, Colorado State University, Fort Collins, CO 80523.

E-mail: kummerow@atmos.colostate.edu

occasional deadly floods. Yet, it often lasts no longer than a few hours at a time. Until the end of 1997, precipitation in the global Tropics was still very uncertain, with large numbers of infrared and passive microwave algorithms providing very diverse estimates. In regard to ''global warming,'' the various large-scale models differed among themselves in the predicted magnitude of the warming, distribution, and amount of tropical precipitation and in the expected regional effects of these temperature and moisture changes. Accurate estimates of tropical precipitation were desperately needed to validate and to gain confidence in these models.

The idea of measuring rainfall from space using a combined instrument complement of passive and active microwave (radar) instruments was generated in the early 1980s. By September 1984, a proposal titled, ''Tropical Rain Measuring Mission,'' was submitted to Dr. J. S. Theon at NASA Headquarters by a team of Goddard Space Flight Center investigators consisting of Drs. G. North, T. T. Wilheit, and O. Thiele. Japan's Communications Laboratory, then headed by Dr. N. Fugono, joined in the activities soon thereafter. Joint aircraft flights with an experimental radar (Meneghini et al. 1992) suggested that instrument accuracy was promising. The low Earth orbit needed to realize such measurements from a spaceborne platform, however, immediately raised concerns regarding the sampling adequacy of such a satellite.

The radar data from the four Global Atmospheric Research Program Atlantic Tropical Experiment ships stationed in the intertropical convergence zone (ITCZ) off Africa in 1974 were used for a series of sampling studies. Several orbits and altitudes were considered. An inclined orbit extending between 35°N and 35°S at 350-km altitude was found to be most suitable. The inclined orbit precessed such that the satellite would overfly a given location at a different time every day with an approximate 42-day cycle. This orbit would allow the documentation of the large diurnal variation of tropical rainfall. The altitude of 350 km was satisfactory from the radar antenna requirements. Shin and North (1988) by the summer of 1986 had showed that in the wet tropical areas the sampling errors for monthly accumulations in $5^\circ \times 5^\circ$ grids would be less than 10%. Shin and North also showed that, with rain data from another satellite such as the Special Sensor Microwave Imager (SSM/I) passive microwave radiometers aboard military satellites, the sampling errors could be cut in half and useful data also could be obtained in drier environments.

Insuring the credibility of space-based measurements of rainfall was also a concern from the onset because of the considerable difficulty of making accurate rain measurements via conventional means. Thus, the need for reliable surface-based observations for validating TRMM satellite measurements was established. The ground validation program that followed included conduction of studies to improve rainfall measurement technology; establishment of ground validation sites consisting of radars, rain gauges, and disdrometers around the Tropics; development and expansion of techniques to measure rainfall in oceanic regions; improvement of ground-based rainfall estimation techniques; and development of radar processing and analysis software for producing and analyzing ground validation (GV) products. To complement the surface-based measurements, the planning for extensive field campaigns was initiated early to provide the necessary microphysical and dynamical structure of convective systems in the Tropics after launch.

TABLE 1. Goals of TRMM established by the Science Steering Group in 1986.

1) To advance the earth science system objective of understanding the global energy and water cycles by providing distributions of rainfall and latent heating over the global Tropics.
2) To understand the mechanisms through which changes in tropical rainfall influence global circulation and to improve ability to model these processes in order to predict global circulations and rainfall variability at monthly and longer timescales.
3) To provide rain and latent heating distributions to improve the initialization of models ranging from 24-h forecasts to short-range climate variations.
4) To help to understand, to diagnose, and to predict the onset and development of the El Niño, Southern Oscillation, and the propagation of the 30–60-day oscillations in the Tropics.
5) To help to understand the effect that rainfall has on the ocean thermohaline circulations and the structure of the upper ocean.
6) To allow cross calibration between TRMM and other sensors with life expectancies beyond that of TRMM itself.
7) To evaluate the diurnal variability of tropical rainfall globally.
8) To evaluate a space-based system for rainfall measurements.

In November of 1985, the first major workshop was convened near Goddard to develop the proposed TRMM further. Many participants from this meeting soon organized into a more formal Science Steering Panel headed by Dr. E. Rasmusson. This group released a report establishing the science priorities for the mission in 1986. These goals are given in Table 1. Although tropical precipitation is organized on the mesoscale, it is noteworthy that the primary objectives of the mission were to improve climate models and to aid them in climate prediction. It was proposed to have a dual-frequency radar, a multichannel dual-polarized, conically scanning passive microwave instrument similar to SSM/I, a single-frequency cross-track scanning radiometer to sample along with the radars, and a visible/infrared radiometer similar to the Advanced Very High Resolution Radiometer. The purpose of the visible/infrared instrument was to enable TRMM to establish the connection between TRMM and operational geostationary platforms and thus to serve as a ''flying rain gauge.'' The dual-frequency radar and radiometer combination would be able to derive high-quality precipitation profiles. The small cloud drops that play an integral part in the latent heat release process, however, would not be observable with sufficient accuracy to construct vertical profiles. It was therefore planned from the start to

TABLE 2. TRMM sensor summary—Rain package.*

Microwave radiometer (TMI)	Radar (PR)	Visible and infrared radiometer (VIRS)
10.7, 19.3, 21.3, 37.0, and 85.5 GHz (dual-polarized except for 21.3: vertical only)	13.8 GHz	0.63, 1.61, 3.75, 10.8, and 12 μm
10 km $\times$ 7 km field of view at 37 GHz	4.3-km footprint and 250-m vertical resolution	2.2-km resolution
Conically scanning (53° inc.)	Cross-track scanning	Cross-track scanning
760-km swath	215-km swath	720-km swath

*Additional instruments belonging to the EOS: CERES and LIS.

use results of a cloud-resolving numerical model in retrieving the important latent heat profiles.

The encouraging results from the sampling and aircraft studies led the National Aeronautics and Space Administration (NASA) Headquarters to select TRMM from a number of competing proposals from atmospheric scientists proposing low-cost atmosphere missions. In 1986, the Japanese Space Commission accepted an invitation to study jointly the feasibility of TRMM. In 1987 NASA designated TRMM as an Earth Probe but decided in the spring of 1988, that the phase-A budget estimate for TRMM exceeded Earth Probe specifications. The Science Steering Group therefore decided to descope the radar to a single frequency at 14 GHz. The cross-track scanning radiometer was also eliminated. In addition, the resolution of the infrared sensor was reduced from 1 to 2 km, and the number of data products planned for the data system was reduced to the minimum needed for rainfall purposes. Agreements between the United States and Japan were formalized in 1988, leading to a new start for a joint U.S.–Japan mission at that time. The Japanese agreed to provide the precipitation radar and a launch by their new HII rocket. NASA would provide the spacecraft and the other rain-sensing instruments. The U.S. Congress passed support for TRMM for a new start in 1991, and the project got under way formally.

At this time, two important decisions were made. The first was to enhance slightly the now single passive microwave radiometer to include a channel at 10 GHz. This addition was important to avoid saturation from the heavy tropical rainfall. The second was to accommodate two Earth Observing System (EOS) instruments, namely, a Lightning Imaging Sensor (LIS) and a Clouds and the Earth's Radiant Energy System (CERES) to measure the total upwelling radiant energy.

In early 1991, the first TRMM U.S. 3-yr Science Team was selected from about 100 proposals (23 members from the United States and 8 foreign members). Many meetings and workshops on algorithms and validation took place in both the United States and Japan, with results to be discussed in the next section. In 1993, the TRMM observatory passed its critical design review and moved into phase C/D of actual observatory construction. In 1994, the United States and Japan simultaneously selected new science teams that would be in place until the launch of TRMM in 1997. Although it was decided that the two teams should operate independently, a Joint TRMM Science Team made up of team leaders from both countries was established to coordinate the efforts of both teams. This joint team has worked effectively since then through the successful launch of TRMM from Tanegashima Island on 27 November 1997 to the present time. Current expectations are for TRMM to remain in orbit until approximately March 2004, at which time the fuel needed to maintain the low Earth orbit is expected to be depleted.

2. TRMM instruments and instrument data

a. The final instrument complement

The final TRMM instrument complement is shown in Table 2. Although neither the second radar frequency nor the cross-track scanning radiometer was included, the extra 10-GHz channel was included on the multifrequency radiometer, greatly strengthening the passive microwave products.

TRMM's precipitation radar (PR) is the first radar designed specifically for rainfall monitoring to operate from space. Although its swath is relatively narrow and it suffers from the same uncertainties for rainfall estimation as do ground-based radars, the TRMM PR has delivered an incredible wealth of detailed rain structure information. Examples include the studies of propagating rainfall structures across land and ocean by Takayabu et al. (1999), the direct observational evidence for the suppression of rainfall by smoke-contaminated clouds done by Rosenfeld (2000), the improvement of passive microwave rainfall retrievals, and methods for potentially using PR as a reference standard to cross calibrate ground-based radars. The passive TRMM Microwave Imager (TMI) instrument, aside from providing the highest-resolution data available to date, also has been used to derive sea surface temperature by a number of investigators (e.g., Wentz et al. 2000). The combination of passive and active sensors has, in turn, allowed researchers to look into further constraining parameters such as the drop size distribution (DSD) (Haddad et al. 1997; Viltard et al. 2000). The visible and infrared scanner (VIRS) instrument, in turn, has been useful to relate the detailed TRMM observations to the more available geostationary satellite data. It also has played a key role in interpreting early results from the CERES instrument.

The instrument characteristics themselves are not treated here, because they are described in detail in the available literature. The core TRMM instrument, PR, TMI, and VIRS are described in Kummerow et al. (1998). The LIS instrument is described in Christian et al. (1992), and the CERES instrument is described by Lee et al. (1998).

Calibrated and earth-located data from the TRMM instruments are referred to as level-1 data. Coding of the level-1 algorithms was performed by the TRMM Science and Data Information System (TSDIS) for the TMI and VIRS and by the National Space Development Agency of Japan (NASDA) for the PR. The only additional product at level 1 is the PR reflectivity. In this algorithm, the radar returned power is converted into reflectivity, the parameter most often used in science applications. In addition to the conversion, a decision is made about the existence of rain in the radar field of view. If no rain is detected, the entire reflectivity column is set to a missing value. This step was done to help to reduce data volumes in compressed file formats. All TRMM products have version numbers that are incremented each time the data are reprocessed to reflect an advancement of the TRMM products. After beginning with version 3 at launch (versions 1 and 2 were prelaunch test codes), the data have been reprocessed to version 4 beginning on 1 September 1998 and to version 5 beginning on 1 October 1999. Two additional reprocessings are planned before the end of the mission.

b. Instrument calibration

1) TMI CALIBRATION

Almost immediately after launch, a calibration problem was detected with the TMI instrument. To obtain a consistent time series of geophysical parameters from SSM/I and TMI, the TMI was intercompared with the SSM/Is. The SSM/Is on *F-11, F-13,* and *F-14* are used for the intercalibration. TMI level-1B data and SSM/I daily 1.0° maps from 10 December 1997 to 24 April 1998 were spatially collocated to within 0.7° and temporally collocated to within 30 min. To compare best the TMI and SSM/I antenna temperatures (T_A), two corrections for instrumental differences were applied. The TMI incidence angle is slightly different (52.75° vs 53.4° for SSM/I) and the TMI water vapor channel is at 21.3 GHz rather than at 22.235 GHz. Thus, the SSM/I T_As must be adjusted to correspond to the TMI incidence angle and frequencies before comparisons can be made. Over the ocean, the magnitude of the incidence angle adjustment is about 1 K; the frequency adjustment can be as large as 10 K. These adjustments are not constant, but depend on the atmospheric transmittance. No adjustment is made to land observations, because 1) the incidence angle and frequency dependence of T_A is small and 2) there are no reliable models for the incidence angle and frequency variation of land observations.

Using collocated T_A, the joint probability density function of $T_{A,\mathrm{TMI}} - T_{A,\mathrm{SSM/I}}$ and $T_{A,\mathrm{SSM/I}}$ was formed for each channel. Results are shown in Fig. 1 that represent the weighted least squares fit to the data. The fit can be expressed in terms of the following equation:

$$T_{A,\mathrm{SSMI}} = a_1 T_{A,\mathrm{TMI}} + a_0. \tag{1}$$

For all channels, the difference between SSM/I and TMI is near zero near $T_A = 295$ K and increases linearly with decreasing T_A. For cold ocean observations, the bias reaches values as high as 5 K. The TRMM rollover maneuver also indicates that $T_{A,\mathrm{TMI}}$ has a warm bias. For comparison, the intercalibration biases for the series of SSM/I platforms were typically only about 0.5 K. Thus the series of SSM/Is showed much better agreement than does TMI.

After some analysis, it was decided to use the following error model:

$$T_{A,\mathrm{TMI}} = (1 - \varepsilon)T_A + \varepsilon T_0, \tag{2}$$

where T_A is the true temperature of the incoming radiation, $T_{A,\mathrm{TMI}}$ is the measurement, T_0 is the physical temperature of some unknown emitter in the field of view (possibly the antenna itself), and ε is the emissivity of that emitter. If one takes the SSM/I observations as truth (with all the appropriate caveats), then (1) and (2) can be combined to obtain the following relationships:

$$\varepsilon = \frac{a_1 - 1}{a_1} \tag{3}$$

$$T_0 = \frac{-a_0}{a_1 - 1}. \tag{4}$$

Thus one can use the SSM/I-versus-TMI comparison to estimate the temperature and emissivity of the error source. Table 3 gives the results. As can be seen, except at 85 GHz, in which we have the least confidence, the emitter temperature is similar to 295 K and the emissivity is about 3%–4%. Because there are no SSM/I-versus-TMI comparisons at 11 GHz, we use the 19-GHz value to specify ε and T_0 at 11 GHz.

Given ε and T_0, (2) can then be used to predict $T_{A,\mathrm{TMI}}$ for the TRMM rollover maneuver for which T_A is equal to 2.7. The predicted difference between $T_{A,\mathrm{TMI}}$ minus 2.7 is given in Table 3 under the column $\Delta T_{A,\mathrm{pred}}$, and the T_A difference that was actually observed is given in the last column. There is generally good agreement between the cold space bias predicted from the SSM/I-versus-TMI comparison and that actually observed, thereby giving us confidence in the error model.

Two corrections are therefore possible to account for the emitting source that appears to be radiating into the TMI feedhorns. The first correction is simply the inverse of (2), where ε and T_0 come from Table 4:

$$T_A = \frac{T_{A,\mathrm{TMI}} - \varepsilon T_0}{1 - \varepsilon}. \tag{5}$$

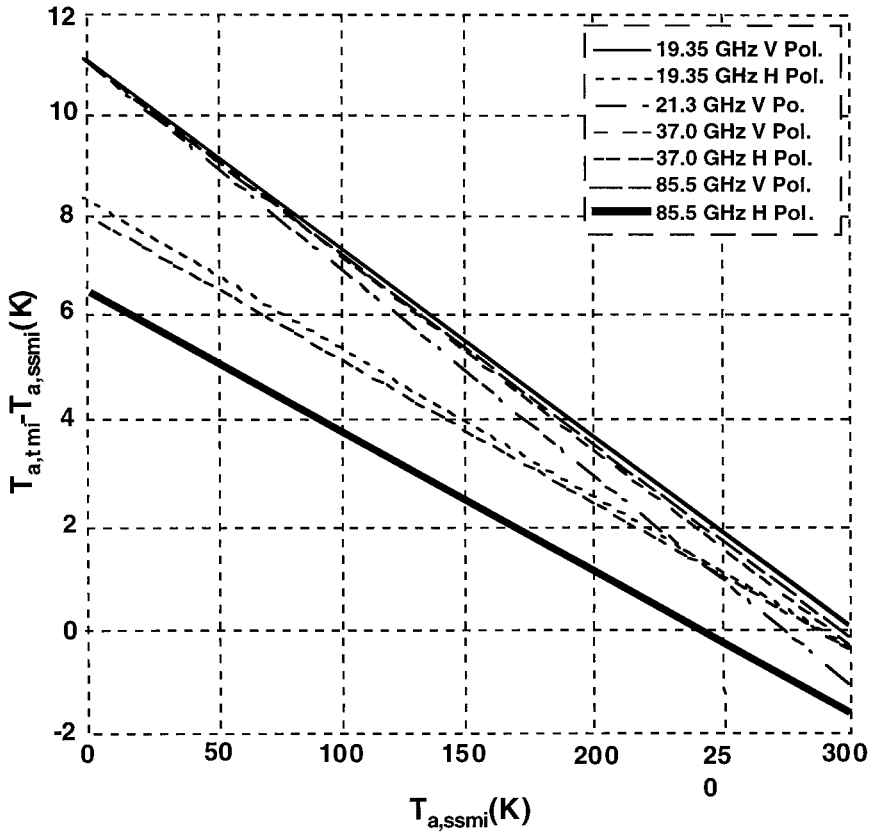

FIG. 1. Regression lines of TMI minus SSM/I T_A difference (ΔT_A) and SSM/I T_A for common SSM/I and TMI channels.

Depending on the application, this correction has the additional advantage that it matches the TMI observations to the SSM/I observations so that one can produce a continuous time series.

The second correction is based on the TRMM rollover maneuver observations and the assumptions that the error model given by (2) is correct and the typical value for T_0 is 295 K. With these assumptions, one has (note $292.3 = 295 - 2.7$)

$$T_A = \frac{292.3T_{A,\mathrm{TMI}} - 295\Delta T_{A,\mathrm{obs}}}{292.3 - \Delta T_{A,\mathrm{obs}}}. \quad (6)$$

Beginning with version 5, the TMI radiance data use the rollover calibration procedure [(6)]. This procedure was done to retain as much physics as possible and to avoid potential errors that can be introduced by simply cross calibrating sensors. Prior data (versions 3 and 4) contain the warm bias error described above.

2) PR CALIBRATION

Accurate calibration of the PR is important to establish the clear interface condition between level-1 and higher-level algorithms, thereby assuring accurate and

TABLE 3. Calibration parameters used for TMI brightness temperature corrections.

Frequency (GHz) and polarization (vertical/horizontal)	ϵ	T_0 (K)	$\Delta T_{A,\mathrm{pred}}$	$\Delta T_{A,\mathrm{obs}}$
11V	0.0370	302.34	11.08	11.1
11H	0.0284	290.41	8.16	9.9
19V	0.0370	302.34	11.08	12.4
19H	0.0284	290.41	8.16	12.3
21V	0.0377	294.64	11.01	13.5
37V	0.0375	296.15	11.02	13.2
37H	0.0274	294.68	8.01	12.2
85V	0.0396	279.61	10.96	13.7
85H	0.0277	239.65	6.57	13.0

TABLE 4. TRMM satellite products.

Name	Reference No.	Purpose
Level-2 data		
Surface cross section	2A21	Radar surface scattering cross section/total path attenuation.
PR rain type	2A23	Type of rain (convective/stratiform) and height of bright band.
TMI profiles	2A12	Surface rainfall and 3D structure of hydrometeors and heating over TMI swath.
PR profiles	2A25	Surface rainfall and 3D structure of hydrometeors over PR swath.
PR–TMI combined	2B31	Surface rainfall and 3D structure of hydrometeors derived from TMI and PR simultaneously.
Level-3 data		
TMI monthly rain	3A11	Monthly 5° rainfall maps—ocean only.
PR monthly average	3A25	Monthly 5° rainfall and structure statistics from PR.
PR statistical	3A26	PR monthly rain accumulations—statistical method.
PR–TMI monthly average	3B31	Monthly accumulation of 2B31 products and ratio of this product with accumulation of 2A12 in overlap region.
TRMM and other satellites	3B42	Geostationary precipitation data calibrated by TRMM, daily, 1° resolution.
TRMM and other data	3B43	TRMM, calibrated IR, and gauge products—data merged into single rain product, monthly, 1° resolution.

stable rain products. To develop the PR calibration algorithm, variation and drift of the PR system parameters are modeled to have ''intermediate-term'' and ''long-term'' components. The former is caused by the temperature change inside the radar and has a period of one orbit (91 rain). The correction for this term can be performed by monitoring the temperature of the instrument. The long-term variations may occur because of gradual degradation of system performance (gain, loss, etc.) and/or failure of some active array elements. To monitor this term, an internal loop-back calibration function, including transmitter power and receiver gain monitors, has been implemented. To conduct an absolute calibration and to detect changes in antenna characteristics and telemetry sensors, a calibration scheme using an external reference target has also been developed.

The internal calibration algorithm has been developed using a detailed PR system model that describes the temperature dependence of all system parameters related to the conversion process from count value to the radar received power or to the radar reflectivity factor. The internal calibration handles the relative intermediate-term variation and some part of the long-term variation through the measurement of the input–output characteristics of the receiver. External calibration of the PR, which handles the absolute calibration and monitoring of long-term variations, is performed using an active radar calibrator (ARC) placed at a ground calibration site in Japan. An error budget analysis of the ARC calibration, including the error in the internal calibration, has indicated that an absolute calibration accuracy of better than 1 dB could be achieved.

In the initial checkout of the PR, which was conducted for 2 months after the TRMM launch, the PR system gain was determined through ARC calibrations. As a result, it was confirmed that the calculated PR receiver gain, based on the data obtained on the ground before launch and using the temperature telemetry, is about 0.6 dB higher than the ARC calibration result, and the PR transmit power is about 0.6 dB lower. Those results were implemented as correction factors to calculate the PR received power and radar reflectivities. They are first implemented in version 5 of the PR level-1 products. Since the completion of the initial checkout, the PR system characteristics have shown excellent stability except for cases where unusual temperature change occurred from power shutdown for satellite maintenance. Both the transmit and receive path gains calibrated by the ARC have shown variations within ± 0.2 dB around the gain initially corrected. Sea surface return levels measured at the incidence angles between 6° and 10° are quite consistent with previous measurements by Ku-band airborne radars developed by the Jet Propulsion Laboratory and Communications Research Laboratory, and have also been stable within about ± 0.2 dB. Moreover, comparisons of PR-measured radar reflectivities of rainfall with those measured at NASA's Florida ground validation site and by the middle and upper atmospheric radar of Kyoto University show good agreements (differences within about 1 dB, on average). Those calibration and validation results indicate that the PR system characteristics have been and will be sufficiently stable and accurate to assure quantitative radar reflectivity and surface radar cross-section measurements.

Such agreement in the observed radar reflectivity has, in turn, forced a much more comprehensive validation strategy to assess the validity of rainfall products. It has also led to unforeseen benefits such as the possibility of using a spaceborne radar as a calibration constant to monitor the multitude of ground-based radars that are calibrated independently and rarely to the 1-dBZ stan-

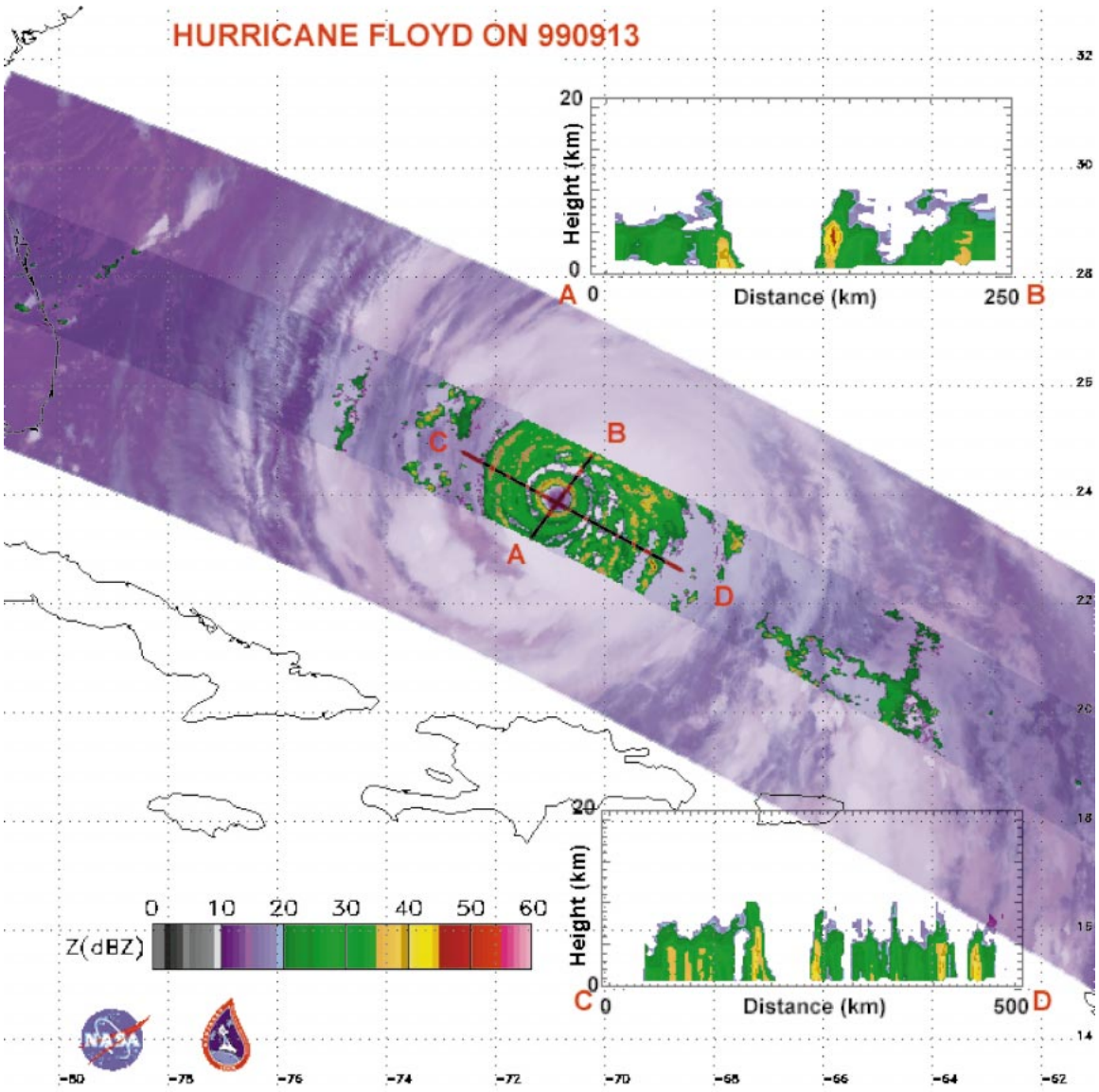

FIG. 2. Hurricane Floyd as captured by the TRMM PR superimposed over a Geostationary Operational Environmental Satellite image. The PR cross sections AB and CD are shown in insets.

dards of the TRMM PR. An example of PR data collected over Hurricane Floyd is shown in Fig. 2.

3) VIRS CALIBRATION

The VIRS radiometric calibration algorithm converts the digital data downlinked from the instrument into spectral radiances. VIRS has five bands, one in the visible, one in the shortwave infrared, (SWIR), and three in the thermal infrared. The calibration algorithm treats each band in the same manner, except that the visible and SWIR bands do not respond to the thermal radiation emitted by the instrument, and these bands do not have the nonlinear responses with input radiance found in the thermal bands. The calibration coefficients for the visible and SWIR bands were determined in the laboratory before launch. VIRS carries a reference blackbody that is used to update the calibration coefficients for the thermal bands for each scan of the instrument on orbit. In addition, VIRS uses an onboard diffuser to view the sun approximately once per month. The VIRS radiometric algorithm uses measurements of these reference sources to provide calibrated spectral radiances for each Earth pixel that it views.

The uncertainties of the VIRS radiances from the visible and SWIR bands are calculated to be 6%. The primary component of these uncertainties, about 5%, comes from the laboratory calibration of the bands. A second component comes from uncertainties in the change of the instrument from its laboratory calibration

to the start of on-orbit operations. The uncertainty contribution from the mirror reflectance (system response vs scan angle) is believed to be small, because the reflectance corrections for these bands are 1% or less. Other instrumental uncertainties are also believed to be small.

The uncertainties for the thermal band radiances are approximately 3%, half those for the visible and SWIR bands. In terms of temperature, the uncertainties are about 2 K at 300 K. The uncertainty in the radiance from the onboard blackbody, combined with the uncertainty in the linearity of the response of the detectors, accounts for two-thirds of the total. On-orbit characterization of response versus scan angle (scan mirror reflectance) has shown differences of up to 2% from the prelaunch values in the thermal infrared bands located at 10.75 and 11.94 μm. However, the use of the on-orbit values does not remove the mirror as a primary source of uncertainty for the VIRS thermal radiance. More detailed information on the VIRS calibration activities may be found in Barnes et al. (2000).

3. TRMM rainfall algorithms

Rainfall products, their error budgets, and the vertical structure of latent heating form the cornerstone of TRMM science. In designing the data systems to generate these products under the very tight budget constraints, it was necessary to minimize the set of products that would satisfy the mission requirements. This section presents an overview of the algorithms deemed to be critical to the mission success. A summary of these products is presented in Table 4 for reference. The levels (2 or 3) follow the standard NASA nomenclature. Level 2 consists of the retrieved geophysical parameters at the satellite footprint level; level-3 products represent either space- or time-averaged geophysical parameters. Like the level-1 products, rainfall products follow the version numbers with version 3 released at launch, version 4 introduced on 1 September 1998, and version 5 introduced on 1 October 1999. Roughly 5 days of data can be reprocessed in 24 h. Reprocessed products are therefore not available immediately, but with some delay depending upon the date the data were collected.

A comprehensive discussion of all the rainfall products is well beyond the scope of this paper. Instead, only the main progress in the rainfall algorithms since launch and the intercomparison between algorithms are presented here. An intercomparison of zonal mean rainfall accumulations for the five major rainfall algorithms (version 4) is presented in Fig. 3. These algorithms represent the at-launch (version 3) algorithms after the initial software errors were corrected (version 4). As can be seen from Fig. 3, the zonal averages for all of 1998 have a wide range between the TMI profiling algorithm and that of the PR. The tropical mean estimates (ocean only) vary from 92 mm month^{-1} for the TMI 2A12 to 61 mm month^{-1} for the PR 2A25 estimate, a range of 31 mm month^{-1}, or 40%. The following short sections describe the initial improvements to the algorithms that have been undertaken during the first two years along with a comparison of the improved algorithms (version 5) that became available on 1 October 1999. The zonal averages for the new versions of the algorithms (version 5) for 1998 are shown in Fig. 4. The version-5 results indicate a narrowing of the differences among the algorithms, with the range over the ocean decreasing to 18 mm month^{-1} (24%). Comparisons of TMI and PR products with surface-based rainfall estimates are discussed in section 4.

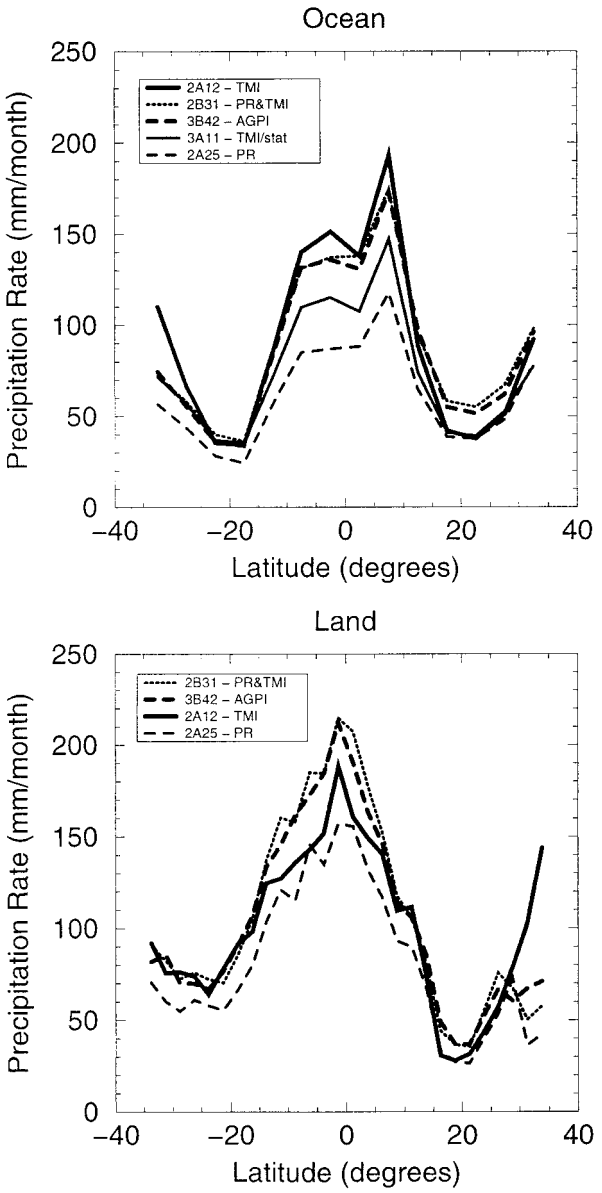

FIG. 3. Zonally averaged mean monthly rainfall for 1998 derived from five independent TRMM rainfall algorithms using the initially corrected at-launch algorithm version (version 4).

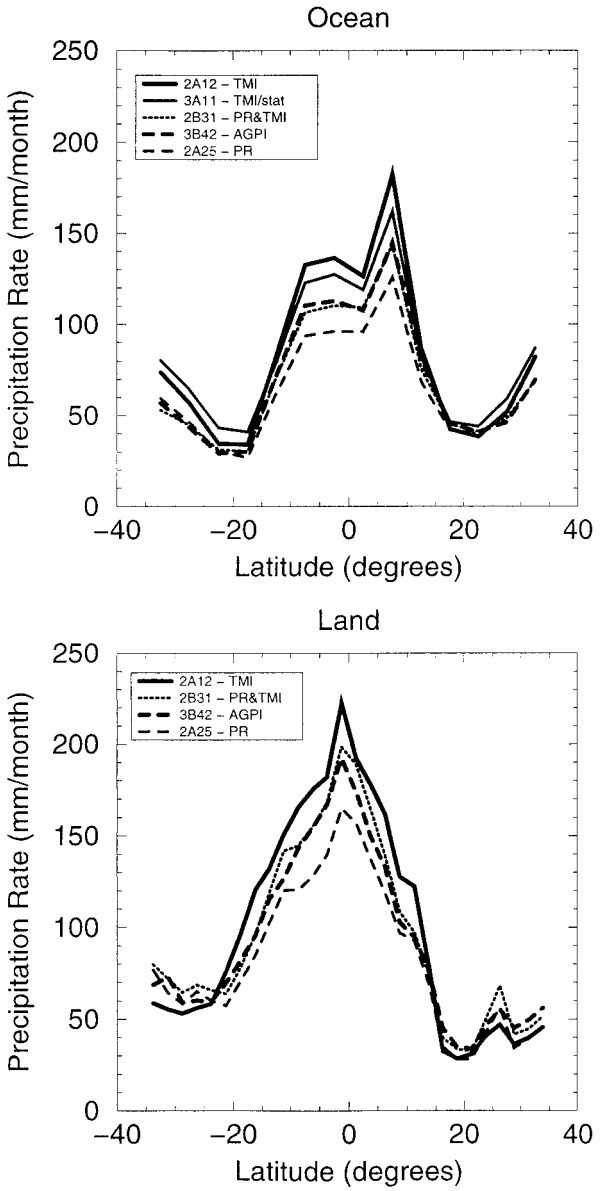

FIG. 4. Zonally averaged mean monthly rainfall for 1998 derived from five independent TRMM rainfall algorithms after the first substantial improvement cycle was implemented on 1 Oct 1999 (version 5).

The annual maps for 1998 resulting from application of the algorithms (version 5) are shown in Fig. 5 at a horizontal spacing of 2.5° latitude–longitude, except for the TMI statistical product, which is only available at 5° spacing over the ocean. The patterns are very similar, with the differences in magnitude following that shown in Fig. 4. Portions of the ITCZ are evident in both hemispheres over the Atlantic and Pacific Oceans, along with land maxima in Africa, South America, and over the ''Maritime Continent.'' Midlatitude maxima are evident across and to the east of Japan and the United States. A rapid transition from El Niño to La Niña rainfall patterns occurred during 1998, producing an annual map somewhat different from the climatological pattern. Adler et al. (2000) describe the evolution of the rainfall pattern during 1998 using TRMM data.

a. TMI profiling algorithm (TSDIS ref. 2A12)

The profiling algorithm being used by TMI makes use of the Bayesian methodology to relate the observed multichannel brightness temperatures to the hydrometeors provided in a preexisting database. This initial database is supplied by nonhydrostatic cumulus-scale cloud models using explicit cloud microphysics. More details can be found in Kummerow et al. (1996). This algorithm was originally developed for the SSM/I and was simply reconfigured for the TMI to take the somewhat different channels and higher spatial resolutions of the TMI into account. The main problem detected with the version-4 TMI algorithm was the algorithm's inability correctly to identify stratiform rainfall far away from any convection. This problem was made worse by the fact that the cloud numerical simulations all have substantial regions of transition clouds between convective and stratiform clouds. These regions are defined as stratiform in the cloud model by virtue of their small vertical wind velocity, but are very inhomogeneous and thus appear more convective to the passive microwave retrieval algorithm. This problem was corrected by requiring that the spatial inhomogeneity of the TMI also resemble the spatial inhomogeneity of the cloud model profiles found in the database. This modification reduced the rainfall rates in clearly stratiform regimes and was the primary reason for a rainfall reduction between versions 4 and 5. In going from version 4 to version 5, the retrieved latent heating has been temporarily deleted. It was found with version 4 that there were some instabilities in the retrieved heating profiles, especially outside the Tropics. It was felt that, until the extratropical latent heating profiles could be generated with confidence, this product should be set to missing. It is planned to reintroduce the latent heating with version 6 of the algorithm.

b. TMI monthly rain mapping algorithm (TSDIS ref. 3A11)

This algorithm produces monthly oceanic rainfall accumulations on a $5^\circ \times 5^\circ$ grid. It also originated as an SSM/I algorithm and has been running successfully with that sensor for over 10 yr. In this algorithm, the brightness temperatures are considered to be a function of only two variables, the rain rate and the height of the 0°C isotherm (freezing level). The freezing level is associated with the total integrated water vapor content (TIWV) through modeling assumptions—namely, that the column water vapor changes from 80% at the surface to saturation at cloud base, which is assumed to be 500

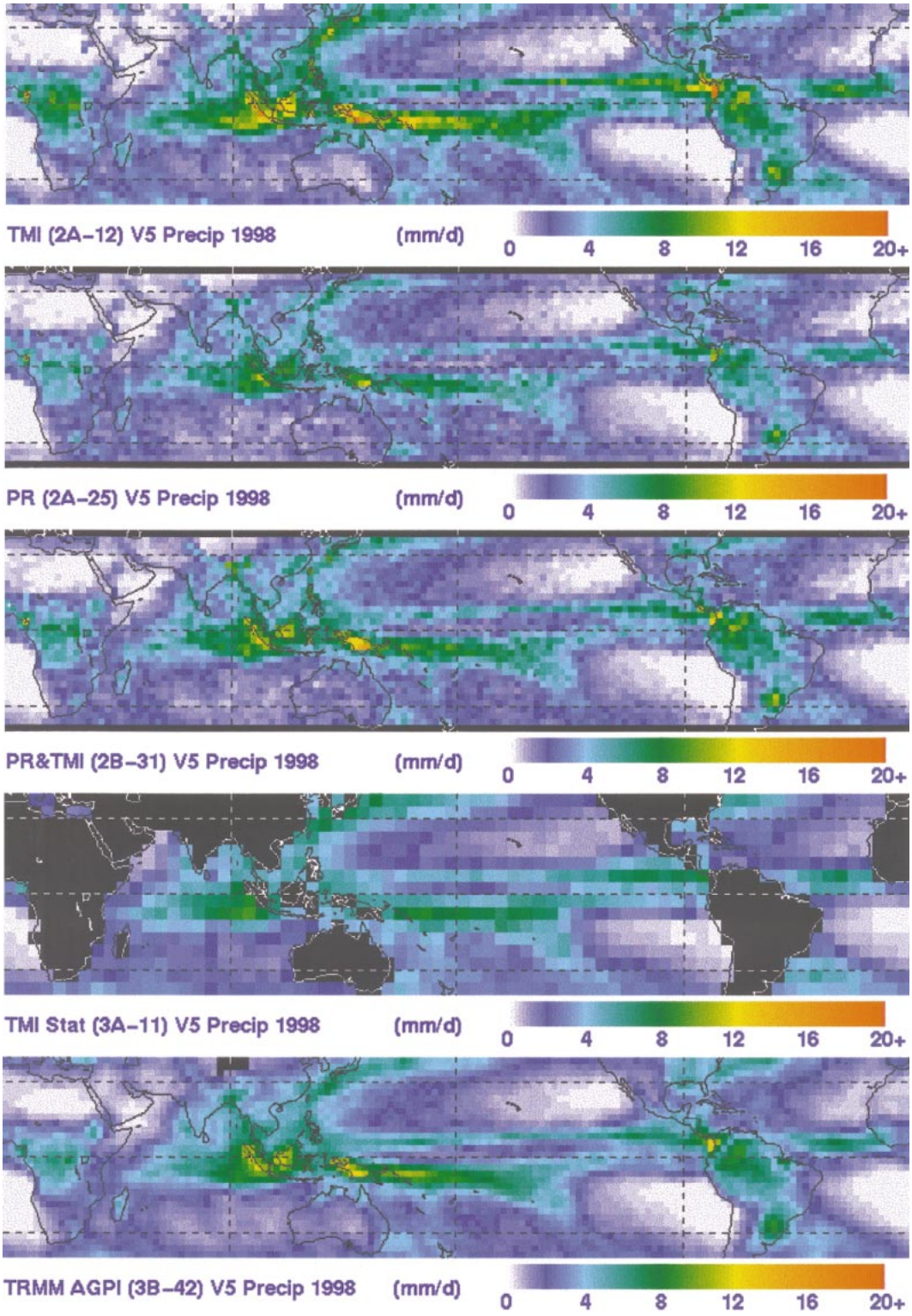

FIG. 5. Rainfall maps (mm month^{-1}) for 1998 (version 5) comparing independent TRMM rainfall estimates.

m below the freezing level. These assumptions, although weak in the general case, are reasonably robust when restricted to raining conditions. Because TIWV affects the 19- and 21-GHz channels very differently, whereas the rain affects them similarly, the two channels can be used to solve for TIWV and, by implication, the freezing level. The rain rate can then be derived using several channel combinations. Because the improved spatial resolution of the TMI can be introduced in a straightforward manner through the beam-filling correction, only minor changes have been made between versions 4 and 5 of this algorithm. A more detailed description of this algorithm and, in particular, comparisons between TMI and SSM/I can be found in Chang et al. (1999).

c. PR profile (TSDIS ref. 2A25)

The rainfall algorithm has undergone a number of changes between version 4 and version 5. Aside from the slight increase in rainfall stemming from the calibration adjustment discussed in section 2b(2), the rainfall algorithm has been modified in three additional ways. The first is an improvement of the algorithm for the estimation of the attenuation at the surface. In the new version, uncertainties in both the radar signals and the surface reference are taken into account.

The second is the replacement of the DSD measured over Darwin, Australia, by a more globally justifiable DSD derived from measured DSDs and radar reflectivity–rainfall rate (Z–R) relations from various places near the ocean all over the world. The third is the introduction of adjustments in the Z–R conversion coefficients that are consistent with the form of the DSD model assumed and the total path attenuation estimate. More details of these procedures can be found in Iguchi et al. (1998). Aside from these algorithm modifications, output data items were slightly changed. Among them, the most important change to the user was the removal of the ambiguities between ''rain-possible'' and ''rain-certain'' classifications flowing down from the level-1 product. In version 4, the algorithm computed rainfall regardless of the rain likelihood, forcing the user to make the determination regarding the likelihood of rainfall. The version-5 algorithm now makes that determination and sets the rainfall to zero if it determines that rainfall is not probable in a rain-possible scenario. The net effect of all these changes has been to increase the rainfall derived by the PR by about 15% on the global scale, with roughly a 10% increase in the convective rainfall and roughly a 20% increase in the stratiform rainfall.

d. Combined PR–TMI profiling algorithm (TSDIS ref. 2B31)

The guiding principle in the design of the ''day-one'' combined algorithms (version 4) was to merge information from the two sensors into a single retrieval that embodied the strengths of each sensor using a very conservative approach in the beginning. The version-4 algorithm designed to run at launch used only the 10-GHz channel of the TMI to obtain an independent estimate of the total path attenuation at 13.8 GHz, the frequency of the TRMM PR. Details of this procedure can be found in Haddad et al. (1997). This conservative approach has now been refined into a scheme that uses all the TMI channels to construct a solution that best fits all the radar and radiometer data. The version-5 algorithm uses the 85-GHz TMI channels to estimate the amount of ice overlying the rain, then uses the appropriate parameterized rain–radiances relations (derived from the TMI profiling algorithm's preexisting database) to find the radar-derived rain profile that best matches the observed radiances. The ''best-match'' criterion is as in Haddad et al. (1997). Details of the rain–radiances relations can be found in Coppens et al. (2000). In addition, the combined PR–TMI algorithm has also resolved the ambiguity caused by the rain-certain and rain-possible conditions introduced by the PR level-1 algorithm.

e. TRMM and other satellite combination (TSDIS ref. 3B42)

The TSDIS algorithm and code for product 3B42 is based on the Adjusted Geostationary Operational Environmental Satellite Precipitation Index technique described by Adler et al. (1994). The technique uses the surface rainfall output from 2A12 with scaling by the ratios in 3B31 (both referenced above) to adjust objectively the rain rates inferred from geo-IR satellite observations and to produce monthly total rain maps for the region of 40°N–40°S. Specifically, the spatially variable ratio is computed between monthly rain-rate averages from coincident 2A12 (with scaling by 3B31 ratios) and VIRS infrared data (1B01), and these monthly ratios are applied to the full 3-hourly geo-IR dataset. In version 4, the algorithm produces a pentad (5 day) product on a 1° latitude–longitude grid. The physics of the algorithm has not changed between version 4 and version 5, but there are some changes in the output product because of changes in the 2B31 algorithm noted above. In addition, the version-5 code generates daily $1° \times 1°$ output files to make it easier for potential users to aggregate data for their individual requirements. Because no additional data were introduced in going from 5- and 30-day products to the daily product, the uncertainty in each daily product has grown proportionally. Figure 5 shows comparisons between the 3B42 product with atoll rain gauge data produced by Morrissey et al. (1995) and the TRMM validation data described in section 4.

f. TRMM and other data combination (TSDIS ref. 3B43)

The TSDIS algorithm and code for product 3B43 are based on the technique described by Huffman et al.

TABLE 5. Description of the primary GV sites. All radars are Dopplerized. Also listed are the number of tipping bucket gauges that measure 1-min rain rates, which have been used in rain map production at Goddard Space Flight Center.

Site	Radar characteristics	No. of gauges
Kwajalein Atoll, Republic of Marshall Islands (8.72°N, 167.73°E)	WSR-93D, 10 cm, polarized	9
Darwin, Australia (12.25°S, 131.04°E)	BMRC/NCAR C-POL, 5 cm, polarized	20
Melbourne, Florida (28.11°N, 80.65°W)	WSR-88D, 10 cm	80
Houston, Texas (29.47°N, 95.08°W)	WSR-88D, 10 cm	80

(1997). Version 4 combines the TRMM and other satellite product (3B42) with the radar–radiometer product (3B31) and a monthly SSM/I product based on the 2A12 algorithm into an intermediate multisatellite product. The scheme is a weighted linear combination done by estimating random errors for each of the input products and then using them to provide weighting by inverse error variance. Version 5 omits the TRMM combined TMI–PR (2B31 above) and SSM/I products because of concerns about diurnal biases. The final combination with the gauge analysis is the same in both versions and again uses a linear combination with inverse error variance weighting.

g. New products developed by TSDIS

TSDIS generates the TRMM standard products and is responsible for distributing data to the TRMM algorithm development team. The Goddard Distributed Active Archive Center (DAAC) performs the broader distribution of data. The interface to both data systems is web based and at the time of writing both can be accessed from the TRMM Web site http://trmm.gsfc.nasa.gov. In Japan, TRMM scientists and associated researchers currently can access these same products through the NASDA data system accessible via http://www.eorc.nasda.go.jp/TRMM.

For the convenience of the algorithm development team, TSDIS also routinely produces subsets of the data products that provide data only over the 10 designated ground validation sites and some additional sites desired by the science team. These subsets have the same format as the regular products but are much smaller. The Goddard DAAC is also making these subsets available to its general users. TSDIS also has a limited capability of producing special subsets for the algorithm development team that can cover regions of the globe other than the TRMM ground validation sites. Such subsets are produced upon request for a specified area and time period.

Because of the early success for the data system, TSDIS has been able to provide expanded product capabilities. In July 1998, TSDIS began generating near–real time data products. The products are the same as the official products described above, but the output data have been reduced drastically to only those parameters that might be of use to the real-time users. This includes surface rainfall and 20 (instead of 80) layers of the PR vertical structure. Unlike the normal data stream that is generated on an orbit-by-orbit basis, the real-time data vary in size depending upon TRMM contact with the data relay satellite. Near–real time data are generally available within 3 h of collection of the oldest bit in the data stream.

In addition to the near–real time data products, TSDIS has also begun distributing gridded surface rainfall data. Global data at 0.5° resolution, as well as land data over South America and Africa, are available at 0.1° resolution. Both datasets contain the rainfall and convective fraction of rain from the TMI, PR, and combined TMI–PR algorithms. The files are produced daily and are written in plain text format for ease of use. The data are written into the grid box that had a TRMM overpass, recording the time of the overpass of the first pixel in that grid box, the rainfall parameters, and the necessary statistics of observations within the grid box to allow for later reconstruction of rainfall accumulations. Further reference on obtaining any of these products currently is available from the TSDIS Web site.

4. Validation efforts during the first two flight years

The validation efforts of TRMM are separated into two categories. The first is the routine comparisons of TRMM satellite rainfall products to operational gauge networks and ground-based radar estimates from a number of cooperative radar sites. The second consists of a series of now completed field experiments around the globe designed to validate physically and, when necessary, to improve the assumptions in both the spaceborne, and the ground-based instrument algorithms. Because cloud dynamical models are used to convert the TRMM observables into latent heating estimates, the field experiments had the additional objective of obtaining datasets that could be used to initialize and to verify these cloud-scale models in diverse meteorological regimes.

a. Climatological validation

Table 5 describes basic characteristics for the four primary validation radar sites. The primary sites cur-

rently are described in detail on the TRMM Web site under ''validation.'' Radar and rain gauge data are provided on a continuous, routine basis to Goddard Space Flight Center. The exception is Darwin, Australia, in which data are received only during the 5–6-month-long wet season. Products from five additional special climatic data sites (Guam, Taiwan, Brazil, Israel, and Thailand) during select, 3–6-month periods of interest to TRMM are currently being generated by investigators at their home institutions.

Generating rainfall products that are of sufficient quality to validate climatological rainfall products from TRMM has been one of the key challenges for the Science Team. Although high-quality radar datasets exist for short periods, it has proven to be very difficult to extend those methodologies to routine operations based upon operational concepts. Data quality has proven to be the most difficult obstacle to overcome, with radar calibration being perhaps the most severe problem. A 1- or 2-dBZ calibration error can translate into error of up to 20% in the rainfall obtained from the application of standard Z–R relations. Although progress has been made to use the TRMM radar itself as a calibration standard, the operational ground-based radar algorithms still use a bulk adjustment procedure to calibrate the monthly radar rainfall products to underlying rain gauge networks. Raw radar data are also contaminated by phenomena such as ground clutter and anomalous propagation, as well as a myriad of nonmeteorological targets such as bugs, birds, chaff, and wildfires. The current quality-control algorithm requires an analyst to inspect manually all radar scans and to vary adjustable parameters to remove these echoes. Rain gauge data also require quality-control procedures and are edited by comparing temporal and spatial correlations with radar-derived rainfall estimates over the locations of the gauges. A procedure has been developed recently to automate this quality-control step (Amitai 1999; Marks et al. 1999), and the algorithm performs well when compared with manual inspection of the merged gauge–radar data. Hereinafter those gauges that pass this quality-control step will be referred to as ''good'' gauges. Numerical experiments have shown improvements of up to 50% when quality-control measures are applied to both the radar and gauge datasets (Kulie et al. 1999; Robinson et al. 1999; Marks et al. 1999).

Rain maps are generated from each of the primary sites by interpolating the raw polar radar data onto Cartesian coordinates with a horizontal spacing of 2 km. Rainfall is classified into convective and stratiform rain according to the horizontal radar reflectivity structure developed by Steiner et al. (1995). For each type of rainfall, the monthly accumulation of the radar pixels (derived using a default relationship of $Z = 300R^{1.4}$, Fulton et al. 1998) directly above each gauge location is compared to the 7-min rain gauge accumulation for the corresponding gauge. A final, gauge-adjusted relationship between Z and rainfall rate R is derived for each site and for each month using

$$Z_i = 300(R_i/G_i)^{1.4}R_i^{1.4}, \tag{7}$$

where R is the total rainfall accumulated by the radar over the locations of the good gauges, G is the rainfall accumulated from tipping-bucket rain gauge data, and the subscript i refers to either convective or stratiform rainfall. Rain rates from gauge and radar data were both accumulated over 7-min intervals, but tests showed that results do not change much for different time intervals. This bulk adjustment is applied to a month of data from each site, with separate Z–R relationships derived for convective and stratiform rainfall. If the total rainfall accumulated over all of the gauges for a month is less than 250 mm, then the bulk adjustment procedure is applied to consecutive months of data.

One last difficulty encountered is the failure of surface radars to operate continuously. Unlike the satellite, for which data gaps can generally be considered to be random, ground-based radar outages can be caused by factors such as severe weather at the radar site. Most often, however, they are caused by routine maintenance activities performed during nonraining periods. Neither of these conditions is random, and therefore they need to be accounted for. Work is underway in using the gauge data to provide area-averaged rain estimates during periods when the radars are not operating. Preliminary results indicate that rainfall underestimation of 10% is possible even when the radar is operational for more than 95% of the period. Implementing this last procedure has taken some time. The first set of products generated routinely by the above procedures for all four primary validation sites were released on 1 June 2000 and are designated as version 3 of the ground validation product. A more rigorous approach would be to compare satellite- and surface-based rainfall estimates only during periods when the radars are operational. This, restriction, however, significantly reduces the sampling to a few rain events per month.

Over oceans, initial comparisons of monthly rain estimates from TMI (2A12) and PR (2A25) have been carried out using estimates from western Pacific Ocean atoll rain gauge data (Morrissey et al. 1995) as shown in Fig. 6. Although the scatter of points is large because of both the sampling errors of TRMM and those of the sparse gauge coverage, the results indicate that the monthly estimates based on the TMI 2A12 algorithm have an overall small negative bias (-10%, Fig. 6a). The monthly estimates based on the PR 2A25 algorithm (Fig. 6b) show a much larger bias (-45%). The somewhat larger scatter of the PR estimates, especially at high rain amounts, may be due to the poorer sampling obtained from the PR's narrower swath.

Over land, the 1998 monthly estimates from TRMM were compared with a gauge-based analysis (Rudolf et al. 1996) in locations (2.5° latitude–longitude boxes) where there are at least two gauges each month (Fig.

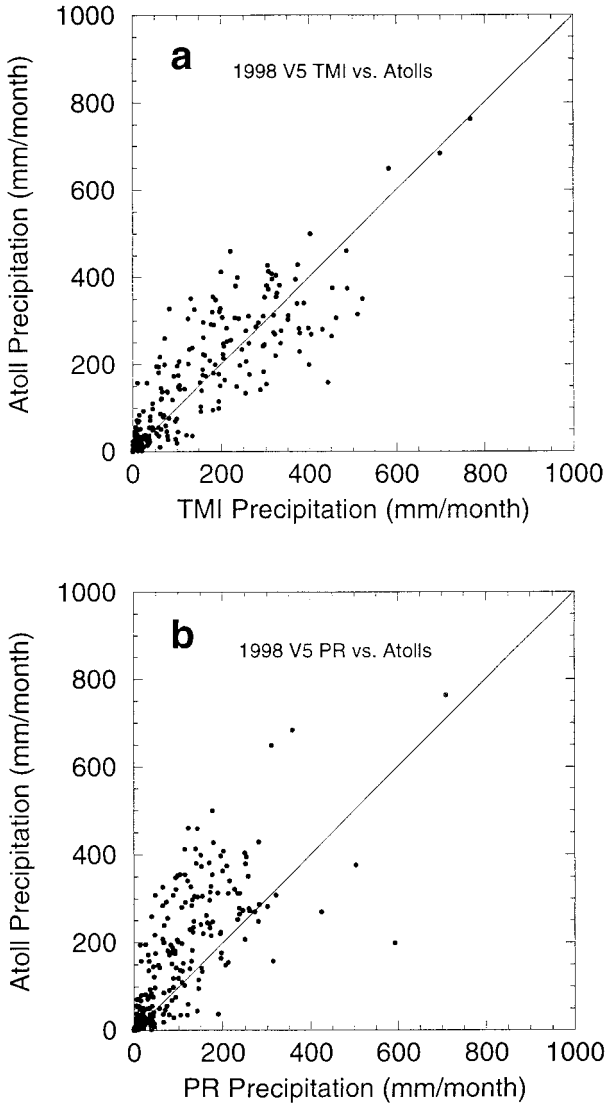

FIG. 6. Comparison of monthly TRMM rainfall estimates with monthly atoll rain gauge data: (a) passive microwave product (2A12), (b) PR product (2A25).

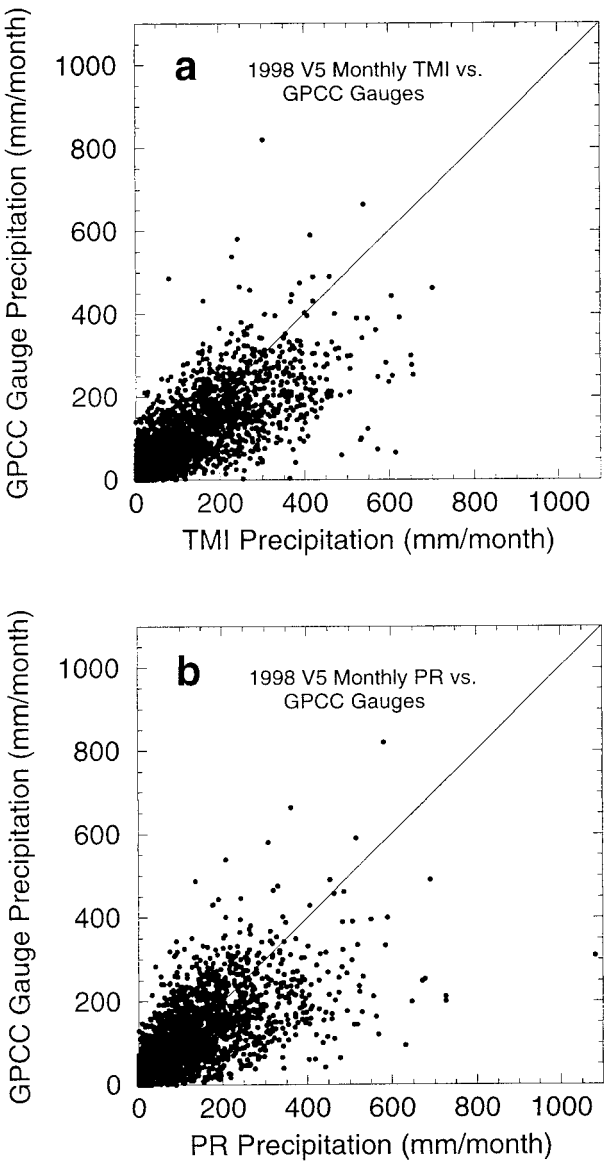

FIG. 7. Comparison of monthly TRMM rainfall estimates with monthly land rain gauge analysis: (a) passive microwave product (2A12), (b) PR product (2A25).

7). Although there is a large scatter of points because of the limited sampling in both the satellite and gauge analyses, the results indicate that both the TMI and PR algorithms have fairly small biases (+16% and +9%, respectively) over the range of the comparison datasets. Both algorithms may show a tendency toward overestimation in areas of high rain amounts, but that feature of the scatter could also be due to the unrepresentativeness in the gauge analysis at high values. The similarity between the TMI and PR results over land in Fig. 7 seems to disagree with the difference indicated in the zonal mean profiles of the various TRMM estimates in Fig. 4. This difference is due to the validation in Fig. 7 being restricted to areas for which gauge information is available, thereby eliminating many of the high–rain amount areas in South America, Africa, and elsewhere. The differences between the TMI and PR results are smaller outside of the heavy rain areas (see Fig. 4). Because these are the areas where the gauge analysis is useful for comparison, the results are biased toward lighter raining areas outside the deep Tropics. Therefore, more detailed validation over land is required to understand fully the algorithm results in different climatological regimes.

In summary, the version-5 TRMM products have converged substantially from the earlier, at-launch products, although there are still substantial differences over ocean and land. Preliminary comparison of TRMM results with existing gauge analyses over land and water

TABLE 6. Summary of TRMM field campaigns. The presence of profilers (P), radiosondes (soundings, S), rain gauges (R), disdrometers (D), tethersonde and surface flux tower (T), and lightning detectors (L) in each experiment are listed in the last column.

Field experiment	Location	No. of radars	No. of aircraft	Other platforms
TEFLUN-A (Texas–Florida Underflight Experiment)	Texas	3	2	D, P, S, R, L
TEFLUN-B (Texas–Florida Underflight Experiment)	Florida	2	2	P, S, R, D, L
SCSMEX (South China Sea Monsoon Experiment)	South China Sea	2	0	S, R, D
TRMM-LBA (TRMM-Large-Scale Biosphere–Atmosphere Experiment in Amazonia)	Rondonia, Brazil	2	2	P, S, R, D, T, L
KWAJEX (Kwajalein Experiment)	Kwajalein, Republic of Marshall Islands	2	3	P, S, R, D, T

indicates that, over water, the more mature TMI-based product compares well with atoll-based rain gauges, and the more experimental PR algorithm produces estimates that are significantly lower than those of the atoll gauges in the western Pacific Ocean. Over land, comparison of both TMI and PR products with gauge analyses produces favorable results with relatively small biases, but questions remain for important areas with high rain amounts that are not represented well in the gauge datasets.

A comparison of some TRMM products with early GV rain maps is shown by Adler et al. (2000). The monthly rain estimates agree to within approximately 20%–40%, which is also the uncertainty among the TRMM algorithms. Because of difficulties discussed earlier, surface radar products also use version numbers to track the continuously improving algorithms and methods. They are, however, not tied to the satellite versions, to avoid the need to validate with products that are changing at the same time intervals. At the time of this writing, version 2 was in effect for the validation products. Version 3 represents a significant improvement in the quality-control procedures, as well as in the interpolation across radar data gaps, which until now were considered to be nonraining. Version 3 was released 1 June 2000 and should reduce biases between satellite- and ground-based radars significantly.

b. Physical validation

Although comparisons among spaceborne algorithms and ground-based products are useful to gain confidence in the various estimates, they cannot be used to reduce uncertainties below the uncertainty in the validation products. Quality-control issues with the GV radar and gauge datasets indicate this uncertainty is approximately 10%–15%. Five field experiments were conducted during the first two years of TRMM to address remaining issues. Although this schedule does not allow much analysis to occur during the experimental phase, it does provide the highest chance of success while the satellite is still operating nominally. Table 6 lists the five different field experiments that were conducted during the first two years of the TRMM mission. These experiments were designed to evaluate the assumptions made by rainfall retrieval algorithms and latent heating estimates made by both the TRMM sensors and the ground-based radars used for the routine validation. Because latent heating is not directly observable, the field experiments collected the necessary atmospheric profile information to initialize and to validate the cloud-resolving models being developed as an independent means of verifying latent heating estimates. In addition to this basic set of objectives, the field experiments were designed as a group to insure that the specific observations could also be compared between experiments so as to gain some insight into the regional dependence of any findings. A number of measurements are therefore common to all experiments.

Based upon the successful completion of the field experiments, three overarching research topics can now be addressed. The first topic is the verification of the satellite's classification of rainfall into convective and stratiform types and the use of appropriate Z–R relations for each type of rainfall. The need to adopt a third, or transition, category is also being investigated. These investigations are being called physical validation. The primary datasets consist of the Doppler dual-polarization radars as well as dual-frequency profilers deployed during each campaign. Backup, or secondary, sensors include ground-based disdrometers and a host of particle probes flying on the microphysics aircraft capable of fully observing the entire DSD spectrum. The second topic is the improvement of the physical modeling of the melting and mixed-phase layers of the clouds. These observations are needed to improve the passive microwave interpretation of the integrated signal reaching the satellite as well as the cloud dynamical model treatment of these regions. The primary data for these studies are the microphysics aircraft underflying the DC-8 or ER-2 aircraft that carried both radars and radiometers to simulate TRMM observations. Enough coincident measurements between the high-altitude aircraft and TRMM were obtained to verify directly the operations of the

instruments designed to simulate the spacecraft. The final topic is the improvement of the cloud dynamical models that ultimately must be used to verify latent heating estimates from both ground-based and satellite sensors. Cloud models primarily need good initial moisture fields. The primary data for this objective are the radiosonde networks that were operated during all campaigns. In addition to the radiosondes, the Large-Scale Biosphere–Atmosphere experiment (LBA) and the Kwajalein Experiment (KWAJEX) also made tower and tethered balloon measurements to observe better the surface fluxes and boundary layer dynamics.

The data needed by the physical validation effort have all been collected and are being analyzed. The dual-polarization radar data were successfully collected during all campaigns except KWAJEX, for which the data have been examined and were found to be unreliable. The profiler data are available for all experiments except the South China Sea Monsoon Experiment (SCSMEX) and are of high quality. Both instruments are being analyzed so that three-dimensional median DSDs can be compared with each other. It is known that these vary from storm to storm and even within a storm (Atlas et al. 1999), but mean statistics over extended time periods are critical for the TRMM algorithms. Results regarding the agreement or disagreement between these two sensors are not yet available. Secondary data from a number of disdrometers, rain gauges, and direct aircraft observations will be used to verify the radar and profiler results. Because of the poor quality of the Kwajalein polarimetric data during the experiment, the profilers and disdrometers have been left on the atoll to make future comparison possible. There is still a large amount of work to be done, but once the mean DSDs have been obtained, these data will then be used directly to test and to improve the satellite assumptions. To validate the satellite products, the DSD information must first be partitioned according to the satellite classification of rainfall (currently into convective and stratiform rain types). Once this partitioning is accomplished, however, direct comparisons between the field experiment results and the satellite products are possible. A number of postexperiment meetings have already been conducted to ensure that the data analysis from individual instruments through to the final comparison with the satellite products occurs in a timely fashion.

The melting-level and mixed-layer microphysics is another area of concentrated attention. The vertical distribution of hydrometeors above the freezing level is a particularly difficult parameter to observe. Cloud-resolving models are a good source of information, but they still give widely disparate pictures of the liquid content in the mixed-phase region just above the freezing level. This disparity, in turn, leads to widely different interpretations of scattering in this region. Aircraft penetrations with simultaneous radar and radiometer observations are the best way to settle the questions. To that end, each experiment (except SCSMEX) has a large number of coordinated flights with coincident radiometric and in situ observations. Because different aircraft probes measure different regions of the drop size spectrum, early efforts by the aircraft microphysics community have centered upon the generation of a uniform dataset that spans the range of drop sizes from 1 μm to 10 mm. Once drop habits and size spectra are quantified, they will be input into radiative transfer models and compared directly with the radiometric observations and cloud dynamical models.

The brightband region is of special interest. In the brightband region, the region just below the freezing level in which the snow melts to form raindrops, the radiometer and radar communities model the attenuation differently. The radiometer community, on the basis of limited evidence, treats the attenuation as being the same as in the rain area below, whereas the radar community treats the bright band as having twice the attenuation of the rain below. During KWAJEX, at least two successful flights were completed with the University of Washington Convair 580 aircraft to study this phenomenon in detail. The Convair aircraft, equipped with an upward-looking radiometer in addition to the standard microphysics probes, flew upward spirals through an extensive brightband region for these experiments. By analyzing the changes in the brightness temperatures and correlating these with the microphysical observations in the bright band, the effect of the bright band on microwave attenuation can be quantified. This work is under way.

The final area of cross-disciplinary interest is in the cloud dynamical modeling. Radiosonde networks were established for each of the field experiments, with soundings taken up to eight times per day at each of up to four sites. In addition to the radiosonde networks, LBA and KWAJEX obtained additional measurements of surface fluxes from tower observations and the boundary layer fluxes from a tethered balloon system. These observations were made with the cloud dynamical models in mind, and various intercomparisons among different sounding systems and soundings with the tethered balloon are under way. The data are being analyzed with attention to quality control and intersensor calibration. The modeling effort is just beginning. One of the key objectives of this modeling effort, however, is to be able to capture differences in climatic regimes so that microphysics and latent heating simulations can eventually be fed back into the algorithms.

The LBA experiment serves as a clear example. Statistically (based on PR analyses), Amazonian convection is less intense on average than the convection over the Congo and north Australia. Analysis from LBA, however, has revealed two well-defined regimes that can be identified in the synoptic and satellite data. Both easterly and westerly regimes exist, as defined by the low-level flow. The westerly regime has many similarities with maritime convection; during easterly phases, Amazonian convection takes on more intense charac-

teristics, similar to the Congo and north Australia. Once the cloud models can capture the observed differences between these regimes (e.g., larger drop sizes and echo tops in the easterly regime), the satellite algorithms can undertake the next level of validation and refinement by treating regimes independently and making use of the latent heating supplied by the improved cloud model simulations to derive better global products.

5. Summary and next steps

Overall, the TRMM mission continues to perform very well. All instruments are operating as expected and have been calibrated to a level necessary for rainfall applications. No further calibration changes except those resulting from normal operations are expected at this time. All rainfall products have been reprocessed through version 5 on the satellite; the ground validation products through version 4 was released 1 June 2000. There are no problems with the satellite itself or the data system. Fuel, which is the limiting resource needed to maintain TRMM's low orbit, is expected to last until approximately March of 2004.

In this paper, we have summarized the latest progress in calibrating TRMM and achieving consistency among TRMM rainfall estimates with each other and ground-based measurements. The initial (version 4) intercomparisons between the TRMM radar and radiometer showed differences of 40% over the global monthly Tropics. Subsequent improvements (version 5) have reduced these differences to 24%, which is also on the order of the uncertainty in the initial version (version 3) of the ground validation products. Current studies of the sensitivity of the radiometers to the melting layer indicate that the radiometer may be slightly overestimating stratiform rainfall, and the PR may be underestimating oceanic rainfall somewhat as compared with the ground-based radar at Kwajalein. The likely cause is an incorrect climatological DSD or an error in the way that point measurements of DSD (made by disdrometers) are being applied to the relative large 4-km footprints of TMI (Nakamura et al. 1998). The field experiment data are being used to address these issues. The Science Teams expect to resolve some of these issues in the near future and have tentatively scheduled the next reprocessing of rainfall products to begin around May of 2001. With insight from the improved validation products and field experiments, algorithms are expected to converge to the 10%–15% level by that time. The Science Team feels that this level is an achievable short-term goal and represents our best knowledge to date. Further agreement between the spaceborne and ground-based sensor will require improved understanding of precipitation physics. It is being actively pursued through the analysis of the field experiment data. These improvements are being targeted for implementation in a final rainfall product reprocessing that is to occur near the end of the mission. Much work remains to be done, but the data, infrastructure, and Science Teams are in place to continue to improve the products and applications in the coming years.

In closing, it is perhaps appropriate to mention that the last NASA planning meeting conducted at Easton, Maryland, in 1999 has endorsed a new concept for global precipitation measurements. The concept is to address climatic rainfall variability and has been formulated with two components. A single primary satellite, similar to TRMM but in a 70° inclination, that can quantify the three-dimensional spatial distribution of precipitation and the associated latent heat release is the first component. This ''core'' platform would carry a dual-frequency rain radar plus a multichannel, polarized passive microwave radiometer akin to TMI. By use of two radar frequencies, it will be possible to determine the first moment of the DSD (i.e., the mode), and thus the quality of rainfall rates may well exceed the quality of standard ground-based weather radars. The radiometer, as is the case for TRMM, would provide further insights into cloud properties and cloud processes beyond that given by radar reflectivities alone and would further serve to transfer knowledge gained by the core satellite to the swaths of complementary satellites that form the second component of the measurement concept. The second component consists of a number of small radiometer satellites (or microsats) flown in a constellation configuration to provide the necessary diurnal sampling needed to force both hydrologic and meteorological models. With a total of eight constellation radiometers, which could consist of a mixture of microsats and various operational satellites carrying passive microwave radiometers (such as SSM/I on Defense Meteorological Satellite Program platforms and the Advanced Microwave Scanning Radiometer on Advanced Earth Observing Satellite-II or Aqua), a sampling frequency of 3 h would be achieved. This sampling rate reduces sampling uncertainties to below 10% for daily rainfall accumulations. As demonstrated with ongoing research related to TRMM, such measurements will have significant positive impacts on prognostic model data assimilation and weather forecasting skills, as well as on hydrological applications that require near-continuous sampling.

Acknowledgments. Any successful program such as TRMM typically owes its success to countless individuals who, with their foresight and dedication, continuously steer a mission in the right direction. Through their efforts, TRMM has been continuously able not only to meet but also to exceed most of the science and engineering goals set forth for this mission. The authors would therefore like to thank, in addition to NASA and NASDA, which made the mission possible, all the individuals that helped to build the satellite and data systems, all the individuals responsible for its safe operations, and all the scientists around the globe for their dedicated efforts.

REFERENCES

Adler, R. F., G. J. Huffman, and P. R. Keehn, 1994: Global tropical rain estimates from microwave-adjusted geosynchronous IR data. *Remote Sens. Rev.,* **11,** 125–152.

——, ——, D. T. Bolvin, S. Curtis, and E. J. Nelkin, 2000: Tropical rainfall distributions determined using TRMM combined with other satellite and rain gauge information. *J. Appl. Meteor.,* **39,** 2007–2023.

Amitai, E., 1999: Dependence of *Z–R* relations on the rain type classification scheme. Preprints, *29th Int. Conf. on Radar Meteorology,* Montreal, Quebec, Canada, Amer. Meteor. Soc., 636–639.

Atlas, D., C. W. Ulbrich, F. D. Marks Jr., E. Amitai, and C. Williams, 1999: Systematic variation of drop size and radar-rainfall relations. *J. Geophys. Res.,* **104,** 6155–6169.

Barnes, R. A., W. L. Barnes, C.-H. Lyu, and J. M. Gales, 2000: An overview of the visible and infrared scanner radiometric calibration algorithm. *J. Atmos. Oceanic Technol.,* **17,** 395–405.

Chang, A. T. C., L. S. Chiu, C. Kummerow, and J. Meng, 1999: First results of the TRMM Microwave Imager (TMI) monthly oceanic rain rate: Comparison with SSM/I. *Geophys. Res. Lett.,* **26,** 2379–2382.

Christian, H. J., R. J. Blakeslee, and S. J. Goodman, 1992: Lightning Imaging Sensor (LIS) for the Earth Observing System. NASA TM-4350, 44 pp. [Available from Center for Aerospace Information, P.O. Box 8757, Baltimore–Washington International Airport, Baltimore, MD 21240.]

Coppens, D., Z. Haddad, and E. Im, 2000: Estimating the uncertainty in passive-microwave rain retrievals. *J. Atmos. Oceanic Technol.,* **17,** 1618–1629.

Fulton, R. A., J. P. Breidenbach, D.-J. Seo, and D. A. Miller, 1998: The WSR-88D rainfall algorithm. *Wea. Forecasting,* **13,** 377–395.

Haddad, Z. S., E. A. Smith, C. D. Kummerow, T. Iguchi, M. R. Farrar, S. L. Durden, M. Alves, and W. S. Olson, 1997: The TRMM ''day-1'' radar/radiometer combined rain-profiling algorithm. *J. Meteor. Soc. Japan,* **75,** 799–809.

Huffman, G. J., and Coauthors, 1997: The Global Precipitation Climatology Project (GPCP) combined precipitation dataset. *Bull. Amer. Meteor. Soc.,* **78,** 5–20.

Iguchi, T., T. Kozu, R. Meneghini, J. Awaka, and K. Okamoto, 1998: Preliminary results of rain profiling with the TRMM precipitation radar. *Proc. Eighth Open Symp. on Wave Propagation and Remote Sensing,* Aveiro, Portugal, International Union of Radio Science Commission F, 147–150.

Kulie, M. S., M. Robinson, D. A. Marks, B. S. Ferrier, D. Rosenfeld, and D. B. Wolff, 1999: Operational processing of ground validation data for the Tropical Rainfall Measuring Mission. Preprints, *29th Int. Conf. on Radar Meteorology,* Montreal, Quebec, Canada, Amer. Meteor. Soc., 736–739.

Kummerow, C., W. S. Olson, and L. Giglio, 1996: A simplified scheme for obtaining precipitation and vertical hydrometer profiles from passive microwave sensors. *IEEE Trans. Geosci. Remote Sens.,* **34,** 1213–1232.

——, W. Barnes, T. Kozu, J. Shiue, and J. Simpson, 1998: The Tropical Rainfall Measuring Mission (TRMM) sensor package. *J. Atmos. Oceanic Technol.,* **15,** 809–816.

Lee, R. B., and Coauthors, 1998: Prelaunch calibrations of the CERES TRMM and *EOS-AM1* spacecraft thermistor bolometer sensors. *IEEE Trans. Geosci. Remote Sens.,* **36,** 1173–1185.

Marks, D. A., M. S. Kulie, M. Robinson, B. S. Ferrier, and E. Amitai, 1999: Standard reference rainfall products used in Tropical Rainfall Measuring Mission ground validation efforts. Preprints, *29th Int. Conf. on Radar Meteorology,* Montreal, Quebec, Canada, Amer. Meteor. Soc., 744–747.

Meneghini, R., T. Kozu, H. Kumagai, and W. C. Boncyk, 1992: A study of rain estimation methods from space using dual-wavelength radar measurements at near-nadir incidence over ocean. *J. Atmos. Oceanic Technol.,* **9,** 364–382.

Morrissey, M. L., M. A. Shafer, S. Postawko, and B. Gibson, 1995: Pacific rainguage data. *Water Resour. Res.,* **31,** 2111–2113.

Nakamura, K., H. Hanado, and K. Furukawa, 1998: A Ground Validation of TRMM PR. *Proc. Symp. on Precipitation Observations from Non-Sun Synchronous Orbit,* Nagoya, Japan, Nagoya University, 245–248.

Robinson, M., D. A. Marks, M. S. Kulie, and B. S. Ferrier, 1999: Seasonal characteristics of nonmeteorological radar reflectivity return in east central Florida and their impact on TRMM ground validation. Preprints, *29th Int. Conf. on Radar Meteorology,* Montreal, Quebec, Canada, Amer. Meteor. Soc., 740–743.

Rosenfeld, D., 2000: Suppression of rain and snow by urban and industrial air. *Science,* **287,** 1793–1796.

Rudolph, B., H. Hauschild, W. Ruth, and U. Schneider, 1996: Comparison of raingauge analyses, satellite-based precipitation estimates, and forecast model results. *Adv. Space Res.,* **18,** 53–62.

Shin, K.-S., and G. R. North, 1988: Sampling error study for rainfall estimates by satellite using a stochastic model. *J. Appl. Meteor.,* **27,** 1218–1231.

Steiner, M., R. A. Houze Jr., and S. E. Yuter, 1995: Climatological characterization of three-dimensional storm structure from operational radar and rain gauge data. *J. Appl. Meteor.,* **34,** 1978–2007.

Takayabu, Y. N., T. Iguchi, N. Kachi, A. Shibata, and H. Kanzawa, 1999: Abrupt termination of the 1997–98 El Niño in response to a Madden–Julian oscillation. *Nature,* **402,** 279–282.

Viltard, N., C. Kummerow, W. S. Olson, and Y. Hong, 2000: Combined use of the radar and radiometer of TRMM to estimate the influence of drop size distributions on rain retrievals. *J. Appl. Meteor.,* **39,** 2103–2114.

Wentz, F., C. Gentemann, D. Smith, and D. Chelton, 2000: Satellite measurements of sea-surface temperature through clouds. *Science,* **288,** 847–850.